ERISNet: Deep learning network for *Sargassum* detection along the coastline of the Mexican Caribbean

Javier Arellano-Verdejo [Corresp., 1] , **Hugo-Enrique Lazcano-Hernandez** [2] , **Nancy Cabanillas-Terán** [Corresp. 2]

[1] Estacion para la Recepcion de Informacion Satelital ERIS-Chetumal, El Colegio de la Frontera Sur, CHETUMAL, QUINTANA ROO, México

[2] Departamento de Ecología y Sistemática Acuática, CONACYT-El Colegio de la Frontera Sur, CHETUMAL, QUINTANA ROO, México

Corresponding Authors: Javier Arellano-Verdejo, Nancy Cabanillas-Terán
Email address: javier.arellano@mail.ecosur.mx, ncabanillas@ecosur.mx

Recently, Caribbean coasts have experienced atypical massive arrivals of pelagic *Sargassum* with negative consequences both ecologically and economically. Based on deep learning techniques, this study proposes a novel algorithm for floating and accumulated pelagic Sargassum detection along the coastline of Quintana Roo, Mexico. Using convolutional and recurrent neural networks architectures, a deep learning network (named ERISNet) was designed specifically to detect this macroalgae along the coastline through remote sensing support. A new dataset which includes pixels values with and without *Sargassum* was built to training and testing ERISNet. Aqua-MODIS imagery was used to build the dataset. After the learning process, the designed algorithm achieves a 90 % of probability in its classification skills. ERISNet provides a baseline for automated systems to accurately and efficiently monitor algal blooms arrivals.

ERISNet: Deep Learning Network for *Sargassum* Detection along the Coastline of the Mexican Caribbean

Javier Arellano-Verdejo[1], Hugo E. Lazcano-Hernandez[2], and Nancy Cabanillas-Terán[2]

[1]**El Colegio de la Frontera Sur, Estación para la Recepción de Información Satelital ERIS-Chetumal, Av. Centenario Km 5.5 C.P. 77014, Chetumal, Quintana Roo, México.**
javier.arellano@mail.ecosur.mx
[2]**Cátedras CONACYT-El Colegio de la Frontera Sur, Chetumal, México;**
hlazcanoh@ecosur.mx, ncabanillas@ecosur.mx

Corresponding author:
Nancy Cabanillas-Terán[2]

Email address: ncabanillas@ecosur.mx

ABSTRACT

Recently, Caribbean coasts have experienced atypical massive arrivals of pelagic *Sargassum* with negative consequences both ecologically and economically. Based on deep learning techniques, this study proposes a novel algorithm for floating and accumulated pelagic *Sargassum* detection along the coastline of Quintana Roo, Mexico. Using convolutional and recurrent neural networks architectures, a deep learning network (named ERISNet) was designed specifically to detect these macroalgae along the coastline through remote sensing support. A new dataset which includes pixels values with and without *Sargassum* was built to training and testing ERISNet. Aqua-MODIS imagery was used to build the dataset. After the learning process, the designed algorithm achieves a 90% of probability in its classification skills. ERISNet provides a baseline for automated systems to accurately and efficiently monitor algal blooms arrivals.

INTRODUCTION

Pelagic *Sargassum* is formed by brown macroalgae *S. fluitans* and *S. natans*, and constitutes floating ecosystems serving as habitats and nurseries for important marine species like sea turtles, fishes, invertebrates, and micro and macro-epiphytes (Rooker et al., 2006; Witherington et al., 2012). However, over the last seven years, Caribbean shores have experienced atypical massive shoals of pelagic *Sargassum*, with exceptional abundances during the summers of 2015 and 2018. Massive influx was observed in numerous Caribbean beaches linked with the accumulation of *Sargassum* spp. (hereafter *Sargassum*)(Gower et al., 2013; van Tussenbroek et al., 2017). Since 2011, these extensive off-shore *Sargassum* shoals have appeared in unprecedented ways in oceanic waters off the coast of northern Brazil (De Széchy et al., 2012; Gower et al., 2013; Sissini et al., 2017). Those shoals likely have origins in the North Equatorial Recirculation Region (NERR) (Schell et al., 2015; van Tussenbroek et al., 2017), suggesting that they did not emerge from the traditional northwestern Atlantic Ocean region known as "The Sargasso Sea". With MODIS (Moderate Resolution Imaging Spectroradiometer) and MERIS (Medium Resolution Imaging Spectrometer) satellite images, it was possible to track a shift in their distribution in order to identify a new possible distribution source (Gower et al., 2013; Sissini et al., 2017).

The biomass reported since 2011 has no precedent (van Tussenbroek et al., 2017; Rodríguez-Martínez et al., 2016). A crucial difference is that *Sargassum* does not remain in the open ocean, but rather washes ashore at the coast. The accumulated biomass has resulted in negative conditions both economically and ecologically (Hu et al., 2016; Schell et al., 2015).

This excessive biomass along the coast due to decomposing *Sargassum* modifies beaches and increases bioerosion, thus having a direct influence on the tourist industry. The accumulation is also associated

46 with physical-chemical water change, anoxia, and generation of hydrogen sulphide (Louime et al., 2017).
47 The decomposition of *Sargassum* biomass on the beaches is a disturbance agent that can also modify the
48 physical, physiological and ecological processes in near-shore coral reef communities. The modified flow
49 of organic matter caused by this disturbance could have negative effects at different scales. The negative
50 effects would also affect tourism, local fisheries (Cuevas et al., 2018; Ferreira et al., 2009; Solarin et al.,
51 2014), and benthic communities. The case of coral reefs is relevant, as they are the most threatened marine
52 ecosystems in the world (Hoegh-Guldberg et al., 2007; Harvey et al., 2018). According to Spalding et al.
53 (Spalding et al., 2017) coral reefs provide nearly US$ 35.8 billion in net benefits of goods and services to
54 world economies each year. This includes tourism, fisheries, and coastal protection. Caribbean region
55 represents US$ 1,853 million of those benefits. Annually around 10 million tourists visit the Mexican
56 Caribbean (Rioja-Nieto and Álvarez-Filip, 2018). Economic loss caused by *Sargassum* arrival can reduce
57 those benefits. In 2015 alone, the state government invested US$ 3 million to remove the macroalgae from
58 tourist areas. More than 4400 workers were hired. In 2018, between June and August US$ 3.1 million
59 were spent on wages for 450 workers.

60 Through spectral water-leaving radiance or surface reflectance, remote sensing has served as the
61 primary means to study ocean constituents suspended or dissolved in water (Dickey et al., 2006). Floating
62 Algae Index (FAI) proposed by Hu et al. in 2009 has been the main method used in remote sensing to
63 assess presence/absence of floating algae in the open sea (Hu, 2009). Specifically, a research has been
64 done to assess and monitor pelagic *Sargassum* in the Western Central Atlantic, Yellow Sea, the Gulf of
65 Mexico, and the Caribbean Sea (Putman et al., 2018). On the other hand, sensors with several spatial,
66 temporal, spectral and radiometric features have been used for the study of *Sargassum* (Dickey et al., 2006;
67 Hu et al., 2015; Cuevas et al., 2018). The use of platforms Aqua-MODIS, Terra-MODIS and Landsat
68 imagery is highlighted due to their wide coverage and worldwide heritage, as well as being open-access
69 datasets (Hu, 2009; Hu et al., 2015; Wang and Hu, 2016). Regarding the coasts of the Gulf of Mexico
70 and the Caribbean Sea, Cuevas et al. (Hu, 2009; Cuevas et al., 2018) presents a methodology to detect
71 *Sargassum* in the northeastern region of the Yucatan peninsula applying the "Random Forest" algorithm
72 to a set of Landsat 8 imagery previously selected. The previous studies are valuable contributions to the
73 detection of floating vegetation like pelagic *Sargassum*. However, no study has dealt with the probability
74 of presence of *Sargassum* along the coastline.

75 From the optical point of view, the oligotrophic waters of the Quintana Roo coasts are transparent
76 under non-sargasso conditions. In 2015 and 2018 specifically, due to the constant arrival of *Sargassum*, its
77 decomposition caused nearshore murky brown waters, which in turn altered the nearshore water surface
78 reflectance values (van Tussenbroek et al., 2017).

79 An Artificial Neural Network (ANN) is a mathematical model inspired by the biological behavior
80 of neurons and how they are organized. The ANNs are massive parallel systems with large numbers of
81 interconnected simple processors. A single layer perceptron (SLP) is a feed-forward network based on a
82 threshold transfer function. SLP is the simplest type of artificial neural network and can only classify
83 linearly-separable cases (Jain et al., 1996). The multilayer Perceptron (MLP) is a generalization of the
84 simple Perceptron and arose as a consequence of the limitations of said architecture in relation to the
85 problem of non-linear separability. Minsky and Papert showed that the combination of several MLPs
86 could be an adequate solution to treat certain non-linear problems (Minsky and Papert, 2017). Neural
87 networks have had many applications in various areas of knowledge such as: control systems (Hunt et al.,
88 1992), business (Vellido et al., 1999), manufacturing (Zhang and Huang, 1995) and medicine (Baxt, 1991)
89 to mention just a few.

90 Deep Learning (DL) was presented in Science magazine in 2006, since then multiple algorithms have
91 been developed, among which convolutional neural network (CNN), recurrent neural network (RNN),
92 stacked auto-encoder (SAE) and deep belief network (DBN). Many variants of deep learning algorithms
93 are a combination of two or more of these algorithms (Zhang et al., 2018).

94 DL is a subfield of machine learning inspired by the ANN and is formed by a set of algorithms
95 that try to model high-level abstractions in data using architectures composed of multiple non-linear
96 transformations (LeCun et al., 2015) In DL, a Convolutional Neural Network (CNN) are a type of ANN
97 composed of multiple layers of convolutional filters of one or more dimensions, and are very effective for
98 tasks of artificial vision, such as classification and segmentation of images (Schmidhuber, 2015).

99 Another type of NN widely used in DL is the Recurrent Neural Network (RNN). An RNN implements
100 a Long Short-term memory architecture (LSTM), which makes RNN an ideal tool for modeling and

2/15

classifying time series (Schmidhuber, 2015). Deep Learning has been used successfully in multiple areas such as biomedicine (Mamoshina et al., 2016), medicine (Greenspan et al., 2016), time series prediction (Weigend, 2018), speech recognition, computer vision, pattern recognition and remote sensing (Liu et al., 2017) among others.

The main objective of this study is to analyze if we can detect *Sargassum* along the Mexican Caribbean coastline by using MODIS data and Deep Learning Networks with an accuracy of more than 80% . Under this view a new algorithm for *Sargassum* detection is presented. This algorithm is based on DL techniques. Hence, our aim was to classify the presence/absence of pelagic *Sargassum* along the coastline of Quintana Roo, Mexico using a NN and MODIS data. This study offers a challenge for remote sensing studies as it allows in the short and mid-term to provide a capable tool to determine variables allowing to detect *Sargassum* pixel by pixel.

MATERIALS AND METHODS

948 km of coastline of the state of Quintana Roo, Mexico was defined as the study area to test and to develop the proposed algorithms. Additionally, by using MODIS satellite information, a set of data containing official information about zones and dates with and without presence of *Sargassum* was also defined.

Study Area

We selected the entire coast of Quintana Roo, located in the eastern zone of the Yucatan Peninsula, Mexico. One-kilometer-sized MODIS pixels in front of the beach line were selected (from 21.496124 Latitude, -87.546677 Longitude, to 18.477211 Latitude, -88.293625 Longitude), bordering the coast of Quintana Roo Figure 1. This region is the main vacation destination in Mexico. In addition, the area is located where massive arrivals of *Sargassum* were recorded in 2015 (van Tussenbroek et al., 2017) and 2018.
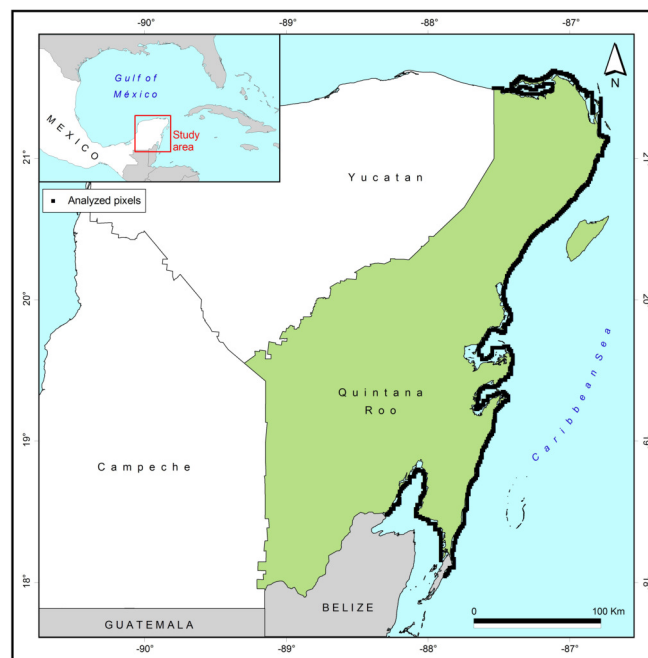

Figure 1. Study Area: Coastal zone of Quintana Roo. Represented by 948 pixels of 1 km^2, close to the beach line.

Dataset Definition and Processing

To build the dataset, three components were developed: 1) A list of sites and dates with and without *Sargassum* based on official information compiled by the government of Quintana Roo (2018) and field work in 2015 and 2018; 2) sets of Aqua-MODIS imagery, both with and without *Sargassum*, for

3/15

127 the coast of Quintana Roo based on the list of dates and sites mentioned above 1; and 3) A software
128 was developed (extract_data.py) to add the list of sites and images set, which ultimately outputs the data set.
129

Area and dates of interest

131 The list of sites and dates with and without *Sargassum* used in this study was built as follows. First, a
132 pixel list of the entire coastal zone of the state of Quintana Roo at a spatial resolution of 1 km was built.
133 This pixel list included the following parameters: latitude, length, position on the x-axis, position on the
134 y-axis, township, and date. With the support of Seadas software*, pixels from an AQUA-MODIS image
135 with WGS84 projection were selected. These 948, one-kilometer-sized pixels represented all of the coast
136 of Quintana Roo[†] Subsequently, based on official information from the state of Quintana Roo[†] and field
137 work, the pixels where *Sargassum* was observed, were labeled. The labeling was done for 29 different
138 dates. A total of 115 different pixels were found with *Sargassum*.

Selection of Aqua-MODIS swath imagery

140 Based on the known *Sargassum* arrivals in the coastal zone of Quintana Roo, Aqua-MODIS swath images
141 were also used in the construction of the dataset. The Julian day and the Universal Time Coordinated
142 (UTC time) of all selected swath images (with and without *Sargassum*) were recorded[‡] and then the PDS
143 files (L0) were downloaded from MODIS OceanData[§]. In total, 80 PDS files were downloaded (42 files
144 corresponding with *Sargassum* dates and 38 files without). After the processing and re-projection of all
145 files, an RGB composition for each swath image was made to allow a visual quality check of each image.
146 Due to the presence of clouds in the area of interest, a total of 19 images were discarded (eight images
147 with *Sargassum* and eleven without). Afterwards, 30 files with *Sargassum* and 29 files without *Sargassum*
148 remained as the imagery used in the development of the dataset. An example of these images is shown in
149 Figure 2. Not all the images were ideal for network training, because of clouds.
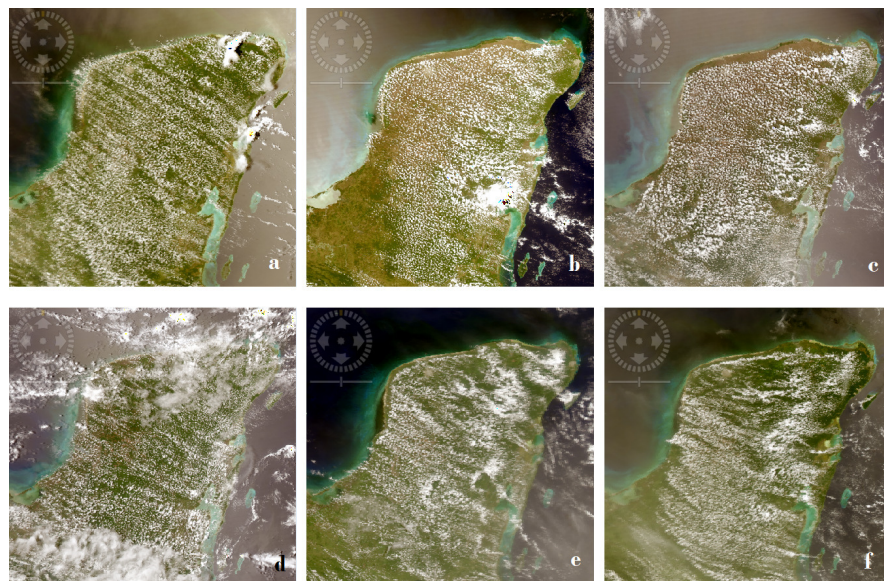

Figure 2. Sample of Aqua-MODIS imagery used in this study, (Day/UTC): a) From 2015 232/18:55,
from 2018: b) 92/19:20, c) 94/19:10, d) 158/19:10, e) 200/19:45 and f) 201/18:50.

Data Processing

151 Data processing started with the swath images (PDS files) downloaded from the ocean color data website[¶].
152 Based on the software SeaDAS7.5.1, PSD file goes through different processing levels to evolve from

---

*https://seadas.gsfc.nasa.gov/
[†]https://www.qroo.gob.mx/noticias/sargazo?buscar=page=0
[‡]https://lance-modis.eosdis.nasa.gov/cgi-bin/imagery/realtime.cgi
[§]https://oceandata.sci.gsfc.nasa.gov/MODIS-Aqua/L0/
[¶]https://oceandata.sci.gsfc.nasa.gov/MODIS-Aqua/L0/

153 level 0 (L0) to level 2 (L2). First, L0 file was processed to obtain the level 1A file (L1A). After that, the
154 file GEO was created. Based in files L1A and GEO, level 1B file (L1B) was produced. Next, L2 product
155 was created and then re-projected. Features of MODIS data processing levels can be consulted on the
156 MODIS Nasa website$^{\parallel}$. Using latitude and longitude pixel-features and the in-house computer program
157 (extract_data.py), rhos and rhot MODIS data corresponding to the coastal zone were extracted. To avoid
158 the Rayleigh scattering, rhos reflectances were used to build the dataset. The wavelength bands selected
159 for this study were: 412, 469, 555, 645, 859, 1240 and 2130 nm. In the Pseudocode 1 the processing
160 workflow is shown.

Pseudocode 1 Scheme of data processing

1: database ← **empty**

2: **for all** L0 datafiles **do**

3:     L1A ← **modis_L1A.py**(L0 file)

4:     GEO ← **modis_GEO.py**(L1A)

5:     L1B ← **modis_L1B.py**(L1A, GEO)

6:     L2 ← **l2gen**(L1B)

7:     Reprojected ← **gpt.sh(L2)**

8:     Data ← **extract_data.py**(Reprojected)

9:     **append_database**(Data)

10: **end for**

11: **return** database

---

161   A database was built with the pixel data of each band for all selected dates. The dataset included 14
162 different attributes and 4515 instances, of which 2306 corresponded to presence of *Sargassum* and 2209
163 without. Additional features are shown in Table 1.

Table 1. Dataset features

Dataset features	
Number of Attributes	14
Data set Characteristics	Multivariate
Attribute Characteristics	Real
Associated Tasks	Classification
Number of Attributes	14
Number of Instances	4515
Number of Clases	2
Number of Instances with *Sargassum*	2306
Number of Instances without *Sargassum*	2209

ERISNet a Deep Learning Network for Sargassum Detection

165 ERISNet is a deep neural network designed to detect *Sargassum* along the coastline. ERISNet is inspired
166 mainly on two types of architectures; Convolutional Neural Networks (CNN) and Recurrent Neural
167 Networks (RNN). An issue present in virtually all models of Machine Learning is overfitting, therefore
168 during the design of the proposed architecture, special attention was paid to maintaining the tradeoff
169 between optimization and generalization of the network by using different mechanisms such as dropout,
170 batch normalization and weight regularization.
171   In Figure 3, the structure of the convolutional block is shown. This block it is formed by four
172 components: Convolutional layer, RELU activation function, Batch Normalization, and Dropout operation.
173   The objective of convolutional blocks is to efficiently extract characteristics or patterns from the
174 input dataset. The main component of the block is a convolutional layer of 1D (dimension one). After
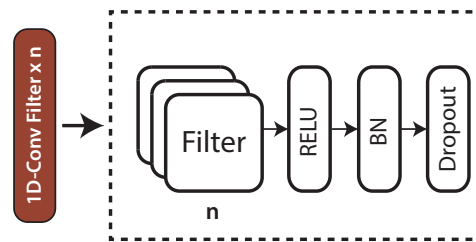

$^{\parallel}$https://modis.gsfc.nasa.gov/data/dataprod/

Figure 3. Convolutional Block

175 conducting numerous tests with different filters and sizes, the decision was made to use a total of [64, 128,
176 128] filters with a size of [8, 5, 3].

177   With the aim of avoiding the overfitting, three mechanisms were used: dropout regularization, weight
178 regularization, and batch normalization. Dropout is one of the most effective and most commonly used
179 regularization techniques for neural networks and is used to improve over-fit on neural networks. At each
180 training stage, individual nodes are either dropped out of the net with probability $1 - p$ or kept in the net
181 with probability p, so that a reduced network is left; incoming and outgoing edges to a dropped-out node
182 are also removed.

183   Weight regularization is another common way to mitigate overfitting. This involved putting constraints
184 on the complexity of a network by forcing its weights to take only small values, making the distribution
185 of weight values more regular. There are two kinds of weight regularization: L1 and L2 regularization.
186 L2 was used in the convolutional blocks of ERISNet. In L2 (see Equation 1) a "squared magnitude" of
187 coefficient as penalty term to the loss function is added.

$$L_2(W) = w_1^2 + w_2^2 + \cdots + w_n^2 \tag{1}$$

188   The convolutional block uses a Batch Normalization operation to increase the network performance.
189 Batch Normalization (BN), is a technique for improving the performance and stability of ANN, providing
190 any layer in a neural network with inputs that are zero mean/unit variance (Ioffe and Szegedy, 2015).
191 During the learning process, the type of initialization of weights could cause a digression to gradients,
192 meaning the gradients have to compensate for the outliers, before learning the weights to produce the
193 required outputs. BN regularizes this gradient by normalizing activations throughout the network. It
194 prevents small changes to the parameters from amplifying into larger and suboptimal changes in activations
195 in gradients.

196   Another component that is part of ERISNet are the recurrent blocks, Figure 4. The main objective
197 of these blocks is to provide memory to the ERISNet. Recurrent neural networks (RNN) are a special
198 type of neural network widely used in problems of prediction in time series. Given their design, the RNN
199 allows information to be remembered for long periods and facilitates the task of making future estimates
200 using historical records. Unlike traditional neural networks, LSTM networks have neuron memory blocks
201 that are connected through layers.These memory blocks facilitate the task of remembering values for long
202 or short periods of time. Therefore, the stored value is not replaced iteratively in time, and the gradient
203 term does not tend to disappear when the retro propagation is applied during the training process.
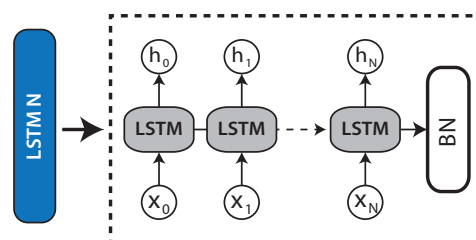

Figure 4. Recurrent block

²⁰⁴ Finally, as in the case of convolutional blocks, recurring blocks also make use of batch normalization to
²⁰⁵ improve network performance. As can be seen in Figure 5, ERISNet consists mainly of nine convolutional
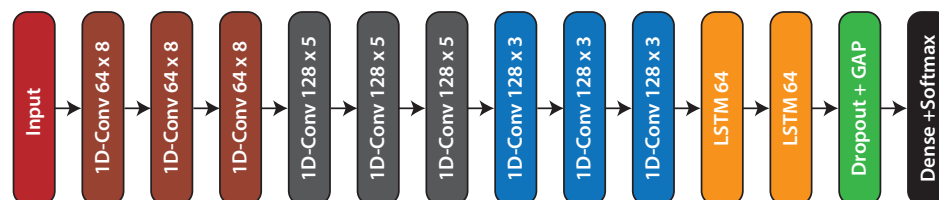²⁰⁶ blocks and two recurring blocks.

Figure 5. ERISNet. *Sargassum* Deep Neural Network.

²⁰⁷ ERISNet was designed using the programming language Python version 3.7.0 and the library Keras
²⁰⁸ 2.2.4 with TensorFlow 1.10.0 as backend.
²⁰⁹ TensorFlow is an open source library developed by the Google Brain Team for numerical calculation
²¹⁰ using data flow graphing programming. The nodes in the graph represent mathematical operations, while
²¹¹ the connections or links in the graph represent the multidimensional data sets (tensors). Tensorflow has
²¹² various automatic learning algorithms and other tools that make it ideal for the development of new
²¹³ methods. Keras is a Python library that provides a clean and simple way to create Deep Learning models
²¹⁴ on top of other libraries such as TensorFlow, Theano or CNTK.
²¹⁵ All the architectures presented in this work were developed and trained using a Lenovo Workstation
²¹⁶ with Intel Xeon EP processor, 64 GB of RAM, NVidia Quadro K5000 GPU running the Linux operating
²¹⁷ system Ubuntu 18.04 64 bits.

RESULTS

²¹⁹ Statistical analysis with the information of bands was performed to evaluate the behavior of the current
²²⁰ dataset. Next, two algorithms extracted from the literature based on neural networks and machine learning
²²¹ are investigated; these algorithms have shown good results when applied to classification problems similar
²²² to that of the present research. Finally, a comparative table is presented with the results of ERISNet and
²²³ the other competitors.

Basic Statistical Analysis

²²⁵ When each of the corrected bands (rhos and rhot) of the generated data with and without *Sargassum*
²²⁶ were averaged, small differences were observed. Only the averages corresponding to bands 859 and
²²⁷ 1240 nm were higher in the case of the presence of *Sargassum*. Therefore, a powerful algorithm-tool is
²²⁸ needed to efficiently classify the small differences among the values of each pixel and thus classify the
²²⁹ presence/absence of *Sargassum*. A basic statistical analysis of data, shows why 859 and 1240 nm are the
²³⁰ bands which FAI index uses. Table 2 shows the means in the case of rhos bands.

Table 2. Mean of the rhos band

	rhos_412	rhos_469	rhos_555	rhos_645	rhos_859	rhos_1240	rhos_2130
Without *Sargassum*	0.131517	0.13489	0.141123	0.124477	0.227052	0.207291	0.085164
With *Sargassum*	0.114489	0.12090	0.133097	0.116607	**0.247237**	**0.233480**	0.084166

²³¹ We have chosen a survey (Wang et al., 2017) showing a wide comparison between different classifica-
²³² tion algorithms by using more than 40 different classic datasets. In those studies, authors propose three
²³³ new classification algorithms based on machine learning techniques and neural networks showing a good
²³⁴ accuracy for the different datasets.
²³⁵ In order to compare the performance of the proposed methodology, we have chosen two effective
²³⁶ algorithms presented in 2017 by Wang et al. In Figures 6 and 8 the two neural networks architectures
²³⁷ used for the comparison are shown.

₂₃₈ **Multilayer Perceptron**

₂₃₉ The multilayer perceptron (MLP) it is defined as the base algorithm for comparison with the rest of the
₂₄₀ proposals. As it can be seen in Figure 6, the MLP used is composed of an input layer, three intermediate
₂₄₁ or hidden layers, and the output layer. Each of the intermediate layers is composed of 500 neurons that
₂₄₂ use the rectified linear unit (RELU) as an activation function. To improve the generalization of the neural
₂₄₃ network, a "dropout" function with values of [0.2 0.2 0.3] respectively has been inserted at the end of
₂₄₄ each of the intermediate layers. Dropout, applied to a layer, consists of randomly dropping out (setting to
₂₄₅ zero) a number of output features of the layer during training. Finally, the network has a softmax layer
₂₄₆ which is widely used in the Multiclass single-layer classification. Formally, each of the blocks of the
₂₄₇ hidden layers it is described as shown in Equation 2.

$$\tilde{x} = f_{(dropout,p)}(x)$$
$$y = W \cdot \tilde{x} + b \qquad (2)$$
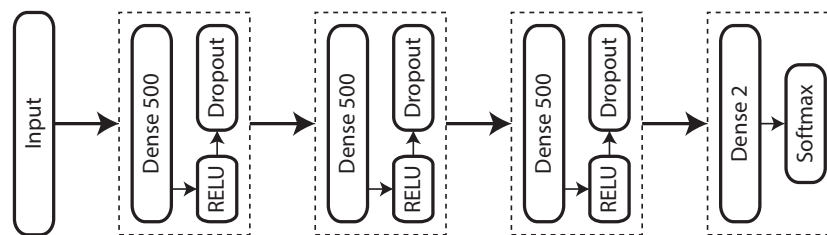$$h = RELU(y)$$

Figure 6. Multilayer perceptron (MLP)

₂₄₈ The MLP was used to perform the classification of the whole dataset (4515 MODIS pixels). The
₂₄₉ dataset was divided in two groups: a training and test group each with approximately the same amount of
₂₅₀ data (see table 4). The learning process was carried out during 3000 epochs, presenting 100 data points in
₂₅₁ each one (batch size). In Figure 7, the result of the learning and test process is shown. On the one hand,
₂₅₂ the continuous line shows that the MLP has a good degree of optimization (close to 100%), which is to be
₂₅₃ expected given the learning capacity of this type of network. On the other hand, the dashed line shows the
₂₅₄ result of the testing process. During the testing process, a set of data which was never used throughout
₂₅₅ the training process was presented to the MLP in order to see the generalization capacity. As shown, the
₂₅₆ MLP has a good level of generalization, correctly classifying 83.76% of the test points. There is a wide
₂₅₇ difference between the optimization and generalization curves, which is usually an indicator of overfitting.
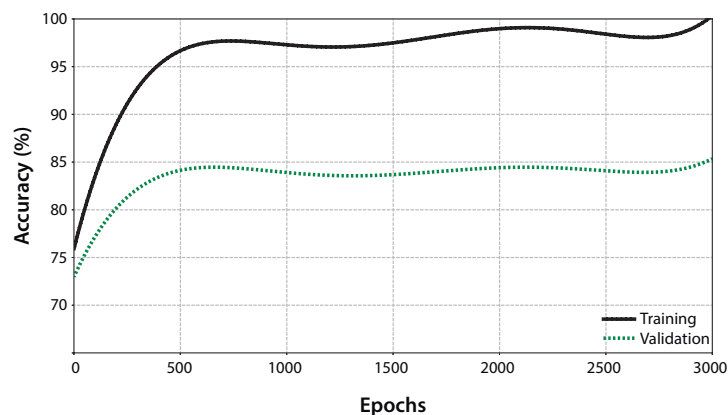

Figure 7. Multilayer perceptron accuracy

8/15

Fully Convolutional Network

Convolutional Neuronal Networks have shown a good performance in classification problems. The fundamental difference between a multilayer perceptron and a convolution layer is that MLP layers learn global patterns in their input feature space whereas convolution layers learn local patterns. The basic block of the FCN is composed of a set of filters that are responsible for the extraction of features from the dataset. RELU has been used as an activation function. At the end of the block, the FCN incorporates a new block called Batch normalization (BN). Batch normalization reduces the amount by which the hidden unit values shift around (covariance shift). To increase the stability of a neural network, BN normalizes the output of a previous activation layer by subtracting the batch mean and dividing by the batch standard deviation, getting ten times or more improvement in the training speed.

In Figure 8, the FCN used is composed of three convolutional blocks: the first block of the network is composed of 128 filters with 8 elements each, the second layer is composed by 256 filters with 5 elements each, and the last block is composed of 128 filters with 3 elements each. The objective of this network is to extract from each of the blocks attributes of the data, from general the particular, thus resulting in a good representation of the information contained in the data. With this representation of the data, it is possible to correctly classify information into different classes. Each of the blocks of the hidden layers are formally described by Equation 3.

$$
\begin{aligned}
y &= W \otimes x + b \\
s &= BN(y) \\
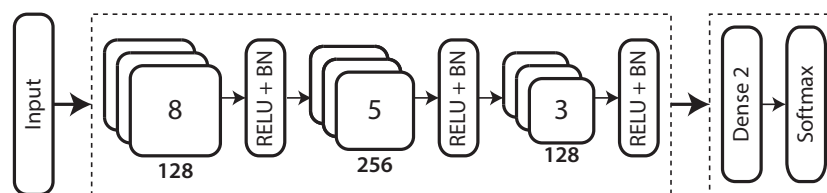h &= RELU(s)
\end{aligned}
\tag{3}
$$

Figure 8. Fully Convolutional Network (FCN)

Like the MLP, the FCN was used to perform the classification of the whole dataset. With the aim of making a comparison on equal terms, both the dataset and the training parameters used for this model were the same as those presented in the MLP. Figure 9 shows the result of the FCN training and testing process. Similarly to the MLP, the FCN had a fairly high level of optimization and the power of generalization showed good results, correctly classifying the 86.38% of the data points. However, the difference between generalization and optimization suggest the possible presence of overfitting in the network once again.
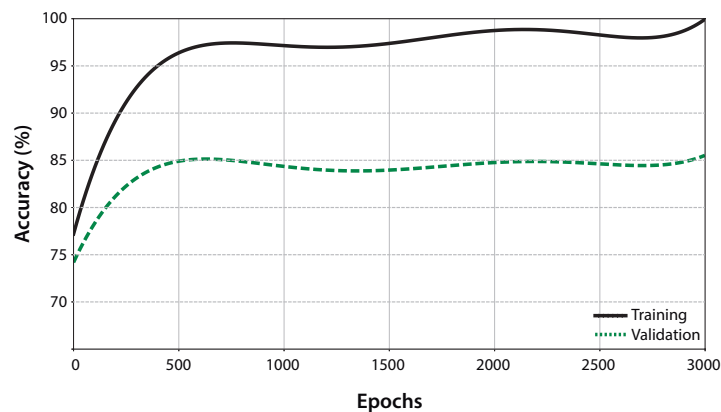

Figure 9. Full convolutional network accuracy

ERISNet Validation

At present there are multiple validation methods for neural networks where cross-validation is the most accepted. Cross validation is a statistical method used to estimate the skill of machine learning models. The cross-validation can be divided mainly into two groups: Exhaustive cross-validation and Non exhaustive cross-validation. Among the methods of Exhaustive cross-validation, the following stand out: Leave one out cross-validation (LOOCV), Exhaustive cross validation, Leave out of cross validation, while Non exhaustive cross validation highlights: k-fold cross-validation, Holdout method and Repeated random sub sampling validation.

Due to the characteristics and size of the dataset used, k-fold was chosen as the cross-validation method of the ERISNet with $k = 5$. Figure 10 shows the k-fold validation scheme for $k = 5$. As observed, the data set was divided into k parts of which $k - 1$ parts were used as a training set, while the remaining part was used as a validation set. In Equation 4, the results of the cross-validation are shown. c_i expresses the number of correct classes within the dataset while e_i corresponds to the number of classes correctly classified by the model.

Training	Training	Training	Training	Testing
Training	Training	Training	Testing	Training
Training	Training	Testing	Training	Training
Training	Testing	Training	Training	Training
Testing	Training	Training	Training	Training

Figure 10. k-fold validation scheme

$$MPCE_k = \frac{1}{k}\sum_{i=1}^{k}\frac{e_i}{c_i} \tag{4}$$

ERISNet was trained, tested, and compared with the rest of its competitors. As in the previous cases, the same criteria were used, that is, the total data set was used by using k-fold cross validation. The algorithm was trained during 3000 epochs with a batch size of 100 data points, the same seed of random numbers used by MLP and FCN was also used. As can be seen in Figure 11, unlike what happened in the case of the MLP and the FCN, the difference between the capacity of optimization and generalization of the network was lower, suggesting that there was no overfitting in the network during the training process. It is important to mention that the level of optimization of the network was less than its competitors, which suggests that if the network is trained during a higher number of epochs this could improve and the generalization could be higher. After the network training, ERISNet obtained a 90.08% success for the classification test points, implying an increase of 7% with respect to the MLP and 4.1% with respect to the FNC.

Figure 12 shows a comparison on the generalization of the MLP, the FCN, and ERISNet. As illustrated, the behaviors of the MLP and the FCN are very similar. However, ERISNet presented an increase in the generalization capacity. Based on all the previous tests, it is concluded that the proposed ERISNet algorithm is capable of classifying more precisely new points than other studies. In Table 3, a summary of the test results is shown.

Table 3. Accuracy results

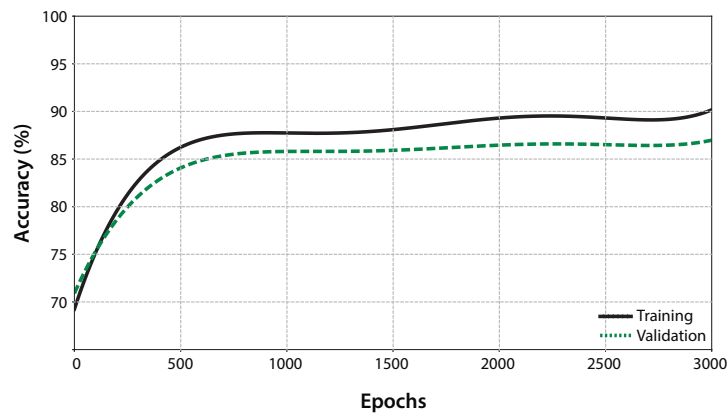|	Mean Accuracy	Best accuracy
ERISNet	**87.23 %**	**90.08 %**
FCN	84.42 %	86.38 %
MLP	83.51 %	83.76 %

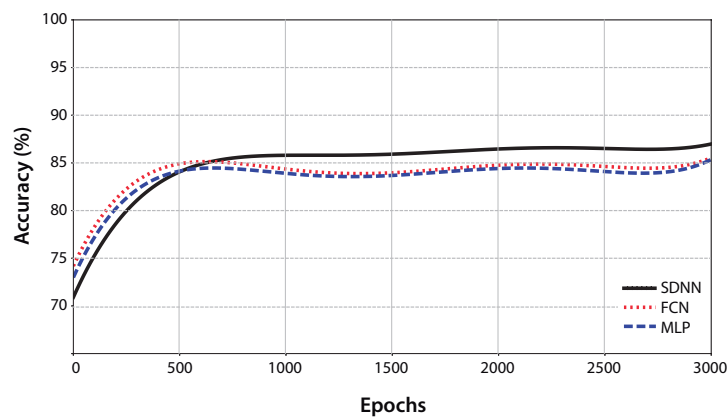**Figure 11.** ERISNet network accuracy

Figure 12. Comparison of the results: *MLP* vs *FCN* vs *ERISNet*

DISCUSSION

This is the first study on *Sargassum* detection along the coastline of the Caribbean Sea. Therefore, there are no algorithms or methodologies that allow us to make a direct comparison between our proposal and other studies. However, as a first step, we have calculated the FAI index to the dataset used in the present study.

FAI Index

Figure 13 shows the boxplot diagram for the FAI index results. A clear statistical difference can be observed between both datasets. It can be seen that the median of the pixels FAI in the presence of *Sargassum* is slightly higher than the median of the pixels without *Sargassum*. The median of the pixels without *Sargassum* is closer to zero.

It is important to note that 50% of the data without *Sargassum* are less compact than that of those with *Sargassum*, which implies a greater distribution of the values within this 50%. The largest difference appears in the lower whiskers of the *Sargassum* boxplot. This difference indicates the FAI value for those points reflects a greater bias with respect to those points without the presence of *Sargassum*. Table 4 shows the results for the calculation of the traditional statistical values made to the FAI index on the data set.

Sargassum detection is a complex issue, for that reason dataset had to be built with official information of dates, sites and with field work. Our dataset is significative to provide remote sensing information about *Sargassum*, until now not available for this region. Hence, it is possible to apply the dataset in other methodologies or for training other algorithms. Thus to compare the classification performance of ERISNet, were chosen two effective algorithms (Wang et al., 2017). As shown in Figure 12, ERISNet obtained the best performance.
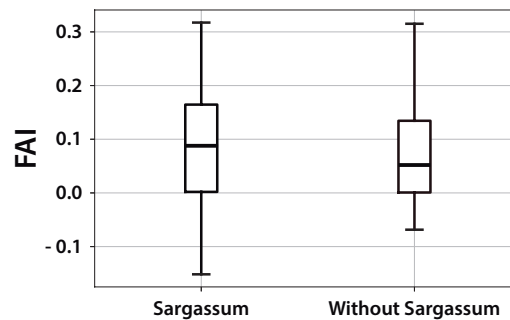
11/15

Figure 13. FAI boxplot for pixels with and without *Sargassum*

Table 4. FAI index for the dataset

	FAI *Sargassum*	**FAI without *Sargassum***
pixels	2306	2209
mean	0.088595	0.072789
std	0.109495	0.081089
min	-0.845114	-0.845114
25%	0.001938	0.000794
50%	0.087812	0.051965
75%	0.164528	0.134386
max	0.317351	0.315139

Sargassum detection along the coastline is a challenge for conventional techniques used in remote sensing. The presence/absence of *Sargassum* on satellite imagery along the coastline is not as clear as in the open sea, because there are several land sea ecosystems. Under these conditions the high classification performance of ERISNet allows to observe the small differences between the values of the bands used for the classification and to determine the presence or absence of *Sargassum* in each pixel with a maximum accuracy of 90.08%. This is highlighted for an ANN, since increase 1% unit in the classification requires high performance design and implementation.

Traditionally, detection of suspended matter in open waters is accomplished through satellite products or through well established indexes (Hu, 2009; Hu et al., 2015, 2016; Cuevas et al., 2018). Therefore, the present study is innovative, since it has a high classification accuracy of pixels with presence/absence of *Sargassum*, using as input data the corrected bands rhos and rhot. The present research showed that under conditions of high concentration of *Sargassum*, as those presented along the coast of Quintana Roo in 2015 and 2018, it was possible to detect *Sargassum* with MODIS data.

Although the coast of the Mexican Caribbean has high economic and ecological importance, there is no a monitoring system that contributes to make decisions against threats of massive arrival of *Sargassum*. Therefore, the present work is very relevant for this region, because offers the basis for an early warning system design.

ERISNet could be applied to other coastal areas of the Caribbean region, thereby we propose to design an artificial neural network capable to detect *Sargassum* in open waters and to build new training datasets based on satellite products and well established vegetation indexes.

CONCLUSIONS

Based on CNN and RNN architectures, ERISNet was developed specifically to detect *Sargassum* along the coastline of Quintana Roo, Mexico. To the best of our knowledge, this is the first method using Deep Learning to detect pelagic *Sargassum* along the coastline that considers not only floating but also accumulated *Sargassum*. Based on Aqua-MODIS swath imagery and well-known sites and dates with and without *Sargassum* along the coastline of Quintana Roo, a dataset was built to train and test all the algorithms used in this study. After the learning process, ERISNet achieved a maximum 90.08% of probability in the classification of pixels with and without *Sargassum*. Additionally, using the dataset for

the present study the FAI index was calculated. The measures of central tendency of the FAI index for data with and without *Sargassum* are clearly different. However that index does not offer a percentage efficiency value pixel-by-pixel. Hence, ERISNet goes further as it offers a quantitative value of its own performance.

Several studies have evaluated the threats that coastal ecosystems of southern Quintana Roo have suffered in the last decades (Alvarez-Filip et al., 2013; Arias-González et al., 2017). However, there is little information that analyzes habitat degradation by *Sargassum*, as it is a relatively new stressor adding to the threats that already exist in the Caribbean. Therefore, an early detection system to alert about massive *Sargassum* arrivals is undoubtedly a challenge for the research of vulnerable coastal zones in the Caribbean, and for the understanding of the threats to these coastal ecosystems.

ACKNOWLEDGMENTS

REFERENCES

Alvarez-Filip, L., Carricart-Ganivet, J. P., Horta-Puga, G., and Iglesias-Prieto, R. (2013). Shifts in coral-assemblage composition do not ensure persistence of reef functionality. *Scientific reports*, 3:3486.

Arias-González, J. E., Fung, T., Seymour, R. M., Garza-Pérez, J. R., Acosta-González, G., Bozec, Y.-M., and Johnson, C. R. (2017). A coral-algal phase shift in mesoamerica not driven by changes in herbivorous fish abundance. *PLoS one*, 12(4):e0174855.

Baxt, W. G. (1991). Use of an artificial neural network for the diagnosis of myocardial infarction. *Annals of internal medicine*.

Cuevas, E., Uribe-Martínez, A., and Liceaga-Correa, M. d. L. Á. (2018). A satellite remote-sensing multi-index approach to discriminate pelagic sargassum in the waters of the yucatan peninsula, mexico. *International Journal of Remote Sensing*, 39(11):3608–3627.

De Széchy, M. T. M., Guedes, P. M., Baeta-Neves, M. H., and Oliveira, E. N. (2012). Verification of sargassum natans (linnaeus) gaillon (heterokontophyta: Phaeophyceae) from the sargasso sea off the coast of brazil, western atlantic ocean. *Check List*, 8(4):638–641.

Dickey, T., Lewis, M., and Chang, G. (2006). Optical oceanography: Recent advances and future directions using global remote sensing and in situ observations. *Reviews of Geophysics*, 44(1):1639.

Ferreira, C. E. L., de Oliveira Ribeiro Junqueira, A., Villac, M. C., and Lopes, R. M. (2009). Marine bioinvasions in the brazilian coast: Brief report on history of events, vectors, ecology, impacts and management of non-indigenous species. In Rilov, G. and Crooks, J. A., editors, *Biological Invasions in Marine Ecosystems: Ecological, Management, and Geographic Perspectives*, pages 459–477. Springer Berlin Heidelberg, Berlin, Heidelberg.

Gower, J., Young, E., and King, S. (2013). Satellite images suggest a new sargassum source region in 2011. *Remote Sensing Letters*, 4(8):764–773.

Greenspan, H., van Ginneken, B., and Summers, R. M. (2016). Guest editorial deep learning in medical imaging: Overview and future promise of an exciting new technique. *IEEE Transactions on Medical Imaging*, 35(5):1153–1159.

Harvey, B. J., Nash, K. L., Blanchard, J. L., and Edwards, D. P. (2018). Ecosystem-based management of coral reefs under climate change. *Ecology and Evolution*.

Hoegh-Guldberg, O., Mumby, P. J., Hooten, A. J., Steneck, R. S., Greenfield, P., Gomez, E., Harvell, C. D., Sale, P. F., Edwards, A. J., Caldeira, K., Knowlton, N., Eakin, C. M., Iglesias-Prieto, R., Muthiga, N., Bradbury, R. H., Dubi, A., and Hatziolos, M. E. (2007). Coral reefs under rapid climate change and ocean acidification. *Science*, 318(5857):1737–1742.

Hu, C. (2009). A novel ocean color index to detect floating algae in the global oceans. *Remote Sensing of Environment*, 113(10):2118–2129.

Hu, C., Feng, L., Hardy, R. F., and Hochberg, E. J. (2015). Spectral and spatial requirements of remote measurements of pelagic sargassum macroalgae. *Remote Sensing of Environment*, 167:229–246.

Hu, C., Murch, B., Barnes, B. B., Wang, M., Maréchal, J.-P., Franks, J., Johnson, D., Lapointe, B. E.,

13/15

Goodwin, D., Schell, J., and Others (2016). Sargassum watch warns of incoming seaweed. *EOS*, 97:10–15.

Hunt, K. J., Sbarbaro, D., Żbikowski, R., and Gawthrop, P. J. (1992). Neural networks for control systems—a survey. *Automatica: the journal of IFAC, the International Federation of Automatic Control*, 28(6):1083–1112.

Ioffe, S. and Szegedy, C. (2015). Batch normalization: Accelerating deep network training by reducing internal covariate shift.

Jain, A. K., Mao, J., and Mohiuddin, K. M. (1996). Artificial neural networks: a tutorial. *Computer*, 29(3):31–44.

LeCun, Y., Bengio, Y., and Hinton, G. (2015). Deep learning. *Nature*.

Liu, W., Wang, Z., Liu, X., Zeng, N., Liu, Y., and Alsaadi, F. E. (2017). A survey of deep neural network architectures and their applications. *Neurocomputing*, 234:11–26.

Louime, C., Fortune, J., and Gervais, G. (2017). Sargassum invasion of coastal environments: a growing concern. *American Journal of Environmental Sciences*.

Mamoshina, P., Vieira, A., Putin, E., and Zhavoronkov, A. (2016). Applications of deep learning in biomedicine. *Molecular pharmaceutics*, 13(5):1445–1454.

Minsky, M. and Papert, S. A. (2017). *Perceptrons: An Introduction to Computational Geometry*. MIT Press.

Putman, N. F., Goni, G. J., Gramer, L. J., Hu, C., Johns, E. M., Trinanes, J., and Wang, M. (2018). Simulating transport pathways of pelagic sargassum from the equatorial atlantic into the caribbean sea. *Progress in Oceanography*, 165:205–214.

Rioja-Nieto, R. and Álvarez-Filip, L. (2018). Coral reef systems of the mexican caribbean: Status, recent trends and conservation. *Marine pollution bulletin*.

Rodríguez-Martínez, R. E., Van Tussenbroek, B., and Jordán-Dahlgren, E. (2016). Afluencia masiva de sargazo pelágico a la costa del caribe mexicano (2014–2015). *Florecimientos Algales Nocivos en México. Ensenada: CICESE*, pages 352–365.

Rooker, J. R., Turner, J. P., and Holt, S. A. (2006). Trophic ecology of sargassum-associated fishes in the gulf of mexico determined from stable isotopes and fatty acids. *Marine Ecology Progress Series*, 313:249–259.

Schell, J. M., Goodwin, D. S., and Siuda, A. N. S. (2015). Recent sargassum inundation events in the caribbean: Shipboard observations reveal dominance of a previously rare form. *Oceanography*, 28(3):8–11.

Schmidhuber, J. (2015). Deep learning in neural networks: An overview. *Neural networks*.

Sissini, M. N., de Barros Barreto, M. B. B., Széchy, M. T. M., de Lucena, M. B., Oliveira, M. C., Gower, J., Liu, G., de Oliveira Bastos, E., Milstein, D., Gusmão, F., Martinelli-Filho, J. E., Alves-Lima, C., Colepicolo, P., Ameka, G., de Graft-Johnson, K., Gouvea, L., Torrano-Silva, B., Nauer, F., Marcos de Castro Nunes, J., Barufi, J. B., Rörig, L., Riosmena-Rodríguez, R., Mello, T. J., Lotufo, L. V. C., and Horta, P. A. (2017). The floating sargassum (phaeophyceae) of the south atlantic ocean – likely scenarios. *Phycologia*, 56(3):321–328.

Solarin, B. B., Bolaji, D. A., Fakayode, O. S., and Akinnigbagbe, R. O. (2014). Impacts of an invasive seaweed sargassum hystrix var. fluitans (borgesen 1914) on the fisheries and other economic implications for the nigerian coastal waters. *IOSR Journal of Agriculture and Veterinary Science*, 7(7):1–6.

Spalding, M., Burke, L., Wood, S. A., Ashpole, J., Hutchison, J., and zu Ermgassen, P. (2017). Mapping the global value and distribution of coral reef tourism. *Marine Policy*, 82:104–113.

van Tussenbroek, B. I., Hernández Arana, H. A., Rodríguez-Martínez, R. E., Espinoza-Avalos, J., Canizales-Flores, H. M., González-Godoy, C. E., Barba-Santos, M. G., Vega-Zepeda, A., and Collado-Vides, L. (2017). Severe impacts of brown tides caused by sargassum spp. on near-shore caribbean seagrass communities. *Marine pollution bulletin*, 122(1-2):272–281.

Vellido, A., Lisboa, P. J. G., and Vaughan, J. (1999). Neural networks in business: a survey of applications (1992–1998). *Expert Systems with applications*.

Wang, M. and Hu, C. (2016). Mapping and quantifying sargassum distribution and coverage in the central west atlantic using MODIS observations. *Remote Sensing of Environment*, 183:350–367.

Wang, Z., Yan, W., and Oates, T. (2017). Time series classification from scratch with deep neural networks: A strong baseline. In *2017 International Joint Conference on Neural Networks (IJCNN)*, pages 1578–1585. ieeexplore.ieee.org.

467 Weigend, A. S. (2018). *Time series prediction: forecasting the future and understanding the past*.
468   Routledge.
469 Witherington, B., Hirama, S., and Hardy, R. (2012). Young sea turtles of the pelagic sargassum-dominated
470   drift community: habitat use, population density, and threats. *Marine Ecology Progress Series*,
471   463:1–22.
472 Zhang, H. C. and Huang, S. H. (1995). Applications of neural networks in manufacturing: a state-of-the-art
473   survey. *The International Journal of Production Research*, 33(3):705–728.
474 Zhang, Q., Yang, L. T., Chen, Z., and Li, P. (2018). A survey on deep learning for big data. *Information*
475   *fusion*, 42:146–157.